Chapter 1

Radioactivity and Alpha Decay

"A factor of 2 in energy means a factor of 10^{24} in half-life! The theoretical explanation of this Geiger–Nuttall rule in 1928 was one of the first triumphs of quantum mechanics."
K. S. Krane [6]

The semi-empirical mass formula and the β-stability parabolas (earlier chapters) predict which nuclei are energetically favoured against nucleon rearrangement. Experiment organises itself differently: on the chart of nuclides, every known species is plotted by neutron number N and proton number Z, and the dominant decay mode in each region is read directly from the map [6, 1, 14, 2]. Heavy nuclei predominantly emit α particles; nuclei far from the valley of β stability adjust N/Z by β decay. This chapter develops the phenomenology of radioactivity and α decay: the chart, the decay Q-value, two-body kinematics, the exponential decay law, the Geiger–Nuttall systematics, and the potential-barrier picture that Gamow used to explain the extreme sensitivity of the half-life to Q.

1.1 Chart of nuclides and where α decay lives

Figure 1.1 shows the chart of nuclides: each point is a known nuclide, with Z on the horizontal axis and N on the vertical axis. Stable species form a narrow band called the *valley of stability*. Away from that band, characteristic decay modes dominate: β^- emission on the neutron-rich side, β^+ emission and/or electron capture on the proton-rich side, and α decay in the upper-right corner where both Z and N are large.

Why heavy nuclei emit α particles. The red-shaded region in Fig. 1.1 corresponds to very heavy nuclei, typically $Z \gtrsim 82$ (lead, bismuth, and the actinides). An α particle is a ^{4}He nucleus ($Z = 2$, $N = 2$). Emitting it reduces both Z and N by 2, moving the system diagonally down and to the left on the chart toward more stable configurations [6, 1].

Three physical reasons combine to favour α emission in this region:

(i) **Coulomb repulsion.** The SEMF Coulomb term grows as $Z(Z-1)/A^{1/3}$. For large Z, the electrostatic energy of packing many protons into a finite volume makes the parent less bound than lighter fragments would be.

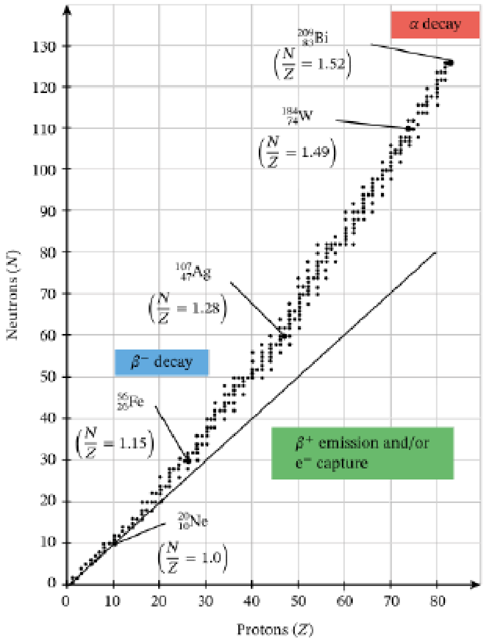

Figure 1.1: Chart of nuclides showing regions of dominant decay mode: α decay, β^- decay, and β^+/electron capture.

(ii) **Declining B/A.** Beyond the iron peak, the average binding energy per nucleon decreases for very heavy nuclei, so releasing a tightly bound cluster can lower the total rest mass.

(iii) **The anomalously large binding of ^{4}He.** Helium-4 is doubly magic ($Z = N = 2$) with experimental binding energy $B_\alpha \approx 28.3\,\text{MeV}$ (about $7\,\text{MeV}$ per nucleon). That large B_α enters the Q-value with a positive sign and makes α emission energetically preferred over most other light clusters [6, 1, 14].

Stable versus long-lived nuclei. Around $A \sim 200$ one finds the heaviest stable nuclides; ^{208}Pb is the heaviest stable nucleus. ^{209}Bi, long treated as stable, is now known to undergo extremely slow α decay. Beyond bismuth no stable species exist; heavy nuclides decay by α and/or β chains toward lead. Many nuclides with $150 < A < 210$ are not strictly stable but are *long-lived*: their α half-lives are long on geological scales; some exceed the age of the Earth, while the primordial uranium isotopes remain because a non-negligible fraction survives (^{238}U, ^{235}U, and ^{232}Th). The chart therefore distinguishes three categories: stable nuclei in the valley, long-lived radioactive nuclei with human-scale or geological half-lives, and short-lived nuclei studied in the laboratory.

Key idea

On the chart of nuclides, α decay occupies the upper-right corner ($Z \gtrsim 82$). Each emission step moves $(A, Z) \to (A - 4, Z - 2)$, equivalently $(N, Z) \to (N - 2, Z - 2)$. ^{208}Pb is the heaviest stable nucleus; the neighboring ^{209}Bi is radioactive but extraordinarily long-lived.

1.2 Particle emission versus fission

When a heavy nucleus breaks apart, the process is classified by the size of the fragments:

- **Particle emission:** one fragment is much smaller than the other (proton, neutron, deuteron, α, or a slightly heavier cluster).
- **Fission:** the nucleus splits into two fragments of comparable mass (treated later in the course).

Among light ejectiles, α emission is usually dominant because $B_\alpha \approx 28.3\,\mathrm{MeV}$ is exceptionally large. Dunlap illustrates this for ^{235}U: emission of a neutron, proton, or ^{3}He has $Q < 0$, while α emission has $Q \approx +4.7\,\mathrm{MeV}$ [1]. Heavier clusters such as ^{12}C or ^{14}C can be emitted in rare instances, but the thicker Coulomb barrier and small preformation probability suppress those channels by many orders of magnitude relative to α decay [6].

1.3 The α decay scheme and Q-value

The basic process is

$$ {}^{A}_{Z}X \;\rightarrow\; {}^{A-4}_{Z-2}Y + {}^{4}_{2}\mathrm{He} + Q. \tag{1.1}$$

The decay is spontaneous only if $Q > 0$: the total rest mass of the products is less than that of the parent, and the excess appears as kinetic energy of the daughter and the α particle.

1.3.1 Q from nuclear masses

Let m_N denote nuclear masses (masses of the bare nuclei, without electrons). Then

$$ Q = \Big[m_\mathrm{N}({}^{A}_{Z}X) - m_\mathrm{N}({}^{A-4}_{Z-2}Y) - m_\mathrm{N}({}^{4}\mathrm{He}) \Big] c^2. \tag{1.2}$$

A positive Q means the parent nucleus is heavier than the sum of the daughter and α masses.

1.3.2 Q from atomic masses: cancellation of electrons

In the laboratory one uses atomic masses m_atom, which include Z electrons for a neutral atom. Write the relation between atomic and nuclear masses as

$$ m_\mathrm{atom}({}^{A}_{Z}X) = m_\mathrm{N}({}^{A}_{Z}X) + Z m_e - \frac{B_e(Z)}{c^2}, \tag{1.3}$$

where m_e is the electron mass and $B_e(Z)$ is the total electronic binding energy of the neutral atom (a few keV per electron, negligible on the MeV scale of nuclear decays).

For the three bodies in Eq. (1.1):

$$ m_\mathrm{atom}({}^{A}_{Z}X) = m_\mathrm{N}({}^{A}_{Z}X) + Z m_e - \frac{B_e(Z)}{c^2}, \tag{1.4}$$

$$ m_\mathrm{atom}({}^{A-4}_{Z-2}Y) = m_\mathrm{N}({}^{A-4}_{Z-2}Y) + (Z-2) m_e - \frac{B_e(Z-2)}{c^2}, \tag{1.5}$$

$$ m_\mathrm{atom}({}^{4}\mathrm{He}) = m_\mathrm{N}({}^{4}\mathrm{He}) + 2 m_e - \frac{B_e(2)}{c^2}. \tag{1.6}$$

Subtract Eq. (1.5) and Eq. (1.6) from Eq. (1.4):

$$\begin{aligned} m_{\text{atom}}({}^{A}_{Z}X) - m_{\text{atom}}({}^{A-4}_{Z-2}Y) - m_{\text{atom}}({}^{4}\text{He}) \\ &= \Big[m_{\text{N}}({}^{A}_{Z}X) - m_{\text{N}}({}^{A-4}_{Z-2}Y) - m_{\text{N}}({}^{4}\text{He})\Big] \\ &\quad + \underbrace{\big[Zm_e - (Z-2)m_e - 2m_e\big]}_{=0} \\ &\quad - \frac{B_e(Z) - B_e(Z-2) - B_e(2)}{c^2}. \end{aligned} \tag{1.7}$$

The electron-mass term vanishes identically because the parent atom has Z electrons, the daughter has $Z-2$, and the helium atom has 2, so $Z = (Z-2) + 2$. The remaining electronic binding-energy difference is of order 10 keV and is neglected in nuclear energetics [1, 6]. Therefore

$$Q \approx \Big[m_{\text{atom}}({}^{A}_{Z}X) - m_{\text{atom}}({}^{A-4}_{Z-2}Y) - m_{\text{atom}}({}^{4}\text{He})\Big]c^2. \tag{1.8}$$

Caution

In Eq. (1.8), $m_{\text{atom}}({}^{4}\text{He})$ is the mass of a *neutral helium atom*, not the mass of the bare α particle. Using the wrong mass tabulation entry is a common source of error of about $2m_ec^2$, with smaller electronic-binding corrections.

1.3.3 Q from binding energies

The binding energy of a nucleus is defined by $m_{\text{N}}c^2 = Zm_pc^2 + Nm_nc^2 - B$. For the decay (1.1), the mass difference can be rewritten entirely in terms of binding energies:

$$\begin{aligned} Q &= \Big[m_{\text{N}}(X) - m_{\text{N}}(Y) - m_{\text{N}}(\alpha)\Big]c^2 \\ &= \Big[\Big(Zm_p + Nm_n - \frac{B_X}{c^2}\Big) - \Big((Z-2)m_p + (N-2)m_n - \frac{B_Y}{c^2}\Big) - \Big(2m_p + 2m_n - \frac{B_\alpha}{c^2}\Big)\Big]c^2. \end{aligned} \tag{1.9}$$

The nucleon mass terms cancel because $A = (A-4) + 4$ and $Z = (Z-2) + 2$:

$$Q = B_Y + B_\alpha - B_X. \tag{1.10}$$

Thus α decay is exothermic when the combined binding of the daughter plus the α exceeds the binding of the parent.

Numerical value of B_α

Evaluated data give $B_\alpha = B({}^{4}\text{He}) \approx 28.296\,\text{MeV}$ [20, 21, 1]. This value should be taken from experiment: the SEMF significantly underbinds the doubly magic ^{4}He and must not be used for B_α.

1.3.4 SEMF estimates and the $A \sim 150$ puzzle

Parent and daughter binding energies can be estimated with the semi-empirical mass formula (pairing term δ often omitted for a first trend):

$$B = a_v A - a_s A^{2/3} - a_c \frac{Z(Z-1)}{A^{1/3}} - a_{\text{sym}} \frac{(N-Z)^2}{A} + \delta. \tag{1.11}$$

Along the β-stable line for fixed A, the atomic number is approximately

$$Z \approx \frac{A/2}{1 + 0.0078\, A^{2/3}}. \tag{1.12}$$

Insert Eqs. (1.11) and (1.12) into Eq. (1.10) with the experimental $B_\alpha = 28.3\,\text{MeV}$. At fixed A, the parent has (A, Z) and the daughter $(A-4, Z-2)$, so

$$\begin{aligned} Q_\alpha^{(\text{SEMF})} &= B(A-4, Z-2) + B_\alpha - B(A, Z) \\ &= a_v\big[(A-4) - A\big] - a_s\big[(A-4)^{2/3} - A^{2/3}\big] \\ &\quad - a_c\left[\frac{(Z-2)(Z-3)}{(A-4)^{1/3}} - \frac{Z(Z-1)}{A^{1/3}}\right] \\ &\quad - a_{\text{sym}}\left[\frac{(N'-Z')^2}{A-4} - \frac{(N-Z)^2}{A}\right] + B_\alpha, \end{aligned} \tag{1.13}$$

with $N = A - Z$ and $N' = A - 4 - (Z-2) = N - 2$. Expanding for large A with Z on the β-stable line (1.12), the volume piece alone contributes $-4a_v$ while the Coulomb release and the fixed B_α win for heavy A. Numerically this estimate crosses $Q_\alpha > 0$ near $A \gtrsim 145$–150.

Yet the chart shows many stable or long-lived nuclides through the lead–bismuth region: ^{208}Pb is the heaviest stable nucleus, whereas ^{209}Bi is an extremely long-lived α emitter. Beyond bismuth one finds no stable species. Two complementary explanations resolve the apparent contradiction:

(i) **Shell and pairing effects.** The SEMF is a smooth average. Individual nuclides can have Q_α shifted by several MeV by shell closures (notably $N = 126$) and odd-even pairing, so some isotopes with SEMF $Q > 0$ are actually sub-threshold or have very small Q [6, 1].

(ii) **$Q > 0$ is necessary but not sufficient.** Even when $Q_\alpha > 0$, the half-life depends exponentially on Q through Coulomb-barrier tunneling (Lecture 17). For $Q \lesssim 4\,\text{MeV}$, lifetimes can exceed 10^{17} s and the decay is effectively unobservable in ordinary laboratory times [1, 6]. A nucleus can therefore have positive α decay energy yet appear stable on human timescales.

Figure 1.2 shows that Q becomes positive for heavy Z near the actinides, with scatter at fixed Z from different N. Adding neutrons to a heavy isotope generally lowers Q_α and lengthens the half-life.

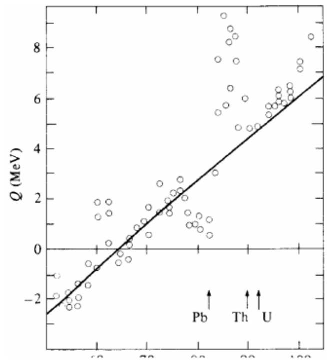

Figure 1.2: Experimental α-decay Q-values (circles) versus proton number Z, compared with the SEMF estimate (solid line). Multiple circles at the same Z correspond to different neutron numbers. Adapted from Cottingham and Greenwood [23].

1.4 Kinematics: sharing of Q between α and daughter

The Q-value is the total kinetic energy released. If the parent nucleus is initially at rest, momentum conservation requires the daughter and α to recoil in opposite directions with equal magnitude of linear momentum.

Step 1: Momentum conservation.

$$\boldsymbol{p}_d + \boldsymbol{p}_\alpha = 0 \quad \Rightarrow \quad |\boldsymbol{p}_d| = |\boldsymbol{p}_\alpha| = p. \tag{1.14}$$

Step 2: Kinetic energies in terms of p.

$$K_d = \frac{p^2}{2M_d}, \qquad K_\alpha = \frac{p^2}{2M_\alpha}, \tag{1.15}$$

where M_d and M_α are the nuclear masses of the daughter and the α particle.

Step 3: Energy conservation.

$$K_d + K_\alpha = Q. \tag{1.16}$$

Step 4: Eliminate p. Substitute the kinetic-energy expressions:

$$\frac{p^2}{2M_d} + \frac{p^2}{2M_\alpha} = Q. \tag{1.17}$$

Factor out $p^2/2$:

$$\frac{p^2}{2}\left(\frac{1}{M_d} + \frac{1}{M_\alpha}\right) = Q. \tag{1.18}$$

Combine the fractions:

$$\frac{1}{M_d} + \frac{1}{M_\alpha} = \frac{M_d + M_\alpha}{M_d M_\alpha}. \tag{1.19}$$

Hence

$$p^2 = \frac{2QM_dM_\alpha}{M_d + M_\alpha}. \tag{1.20}$$

Step 5: Solve for K_α and K_d.

$$K_\alpha = \frac{p^2}{2M_\alpha} = \frac{2QM_dM_\alpha}{M_d + M_\alpha} \cdot \frac{1}{2M_\alpha} = Q\,\frac{M_d}{M_d + M_\alpha}. \tag{1.21}$$

Similarly,

$$K_d = Q\,\frac{M_\alpha}{M_d + M_\alpha}. \tag{1.22}$$

Step 6: Approximate for heavy nuclei. For $A \gg 4$, $M_d \approx (A-4)u$ and $M_\alpha \approx 4u$, so $M_d + M_\alpha \approx Au$. Therefore

$$K_\alpha \approx Q\left(1 - \frac{4}{A}\right), \qquad K_d \approx Q\,\frac{4}{A}. \tag{1.23}$$

For $A = 200$, $K_\alpha/Q = 1 - 4/200 = 0.98$: about 98% of the energy is carried by the α particle and about 2% by the recoiling daughter [6, 1]. Detectors measure K_α; from it one reconstructs $Q = K_\alpha(M_d + M_\alpha)/M_d$.

Remark

The recoiling daughter ($\sim 100\,\mathrm{keV}$ for $Q \sim 5\,\mathrm{MeV}$) has enough energy to break chemical bonds, so α sources must be thin coatings if one wishes to avoid recoil losses from the active layer [6].

1.5 Exponential decay law, activity, mean life, and half-life

Radioactive decay is a Poisson process: for a single nucleus that has not yet decayed at time t, the probability to decay in the next interval $\mathrm{d}t$ is $\lambda\,\mathrm{d}t$, where λ is the decay constant (probability per unit time).

Step 1: Differential equation for $N(t)$. For a large sample, the rate of change of the number of undecayed nuclei is proportional to the number present:

$$\frac{\mathrm{d}N}{\mathrm{d}t} = -\lambda N(t). \tag{1.24}$$

Step 2: Solve the equation. Separate variables and integrate from $t = 0$ (when $N = N_0$):

$$\int_{N_0}^{N(t)} \frac{\mathrm{d}N}{N} = -\lambda \int_0^t \mathrm{d}t \quad \Rightarrow \quad \ln\frac{N(t)}{N_0} = -\lambda t \quad \Rightarrow \quad N(t) = N_0\,e^{-\lambda t}. \tag{1.25}$$

Step 3: Mean life. The mean (average) lifetime of a nucleus in the sample is

$$\tau = \int_0^\infty t\,\lambda e^{-\lambda t}\,\mathrm{d}t = \frac{1}{\lambda}. \tag{1.26}$$

(One integration by parts gives $\tau = 1/\lambda$.)

Step 4: Half-life. The half-life $t_{1/2}$ is defined by $N(t_{1/2}) = N_0/2$:

$$\frac{N_0}{2} = N_0\, e^{-\lambda t_{1/2}} \quad \Rightarrow \quad e^{-\lambda t_{1/2}} = \frac{1}{2} \quad \Rightarrow \quad \lambda t_{1/2} = \ln 2. \tag{1.27}$$

Therefore

$$t_{1/2} = \frac{\ln 2}{\lambda} = \frac{0.693}{\lambda}, \qquad \tau = \frac{t_{1/2}}{\ln 2} \approx 1.443\, t_{1/2}. \tag{1.28}$$

Step 5: Activity. The activity (decay rate) is

$$\mathcal{A}(t) = -\frac{\mathrm{d}N}{\mathrm{d}t} = \lambda N(t) = \lambda N_0\, e^{-\lambda t}. \tag{1.29}$$

Activity also falls by a factor of two in one half-life. In SI units, $\mathcal{A}$ is measured in becquerels (Bq = decays per second); the curie ($1\,\mathrm{Ci} = 3.7 \times 10^{10}\,\mathrm{Bq}$) remains common in nuclear medicine [13, 6].

Key idea

Two laboratory observables characterise α decay: Q (from K_α and kinematics) and $t_{1/2}$ (from the time dependence of activity). They are related by the Geiger–Nuttall rule, explained by Gamow tunneling in Lecture 17.

1.6 Geiger–Nuttall rule

In 1911, Geiger and Nuttall discovered empirically that α emitters with large disintegration energy have short half-lives, and conversely [6, 2]. For known α emitters, Q spans roughly 4–9.5 MeV while $t_{1/2}$ spans from microseconds to $\sim 10^9$ years. The empirical relation is

$$\log_{10}(t_{1/2}/\mathrm{s}) = a\, Q^{-1/2} + b, \tag{1.30}$$

where a and b depend primarily on Z. Different isotopic chains (e.g. thorium, uranium) form parallel lines on the plot.

Even–even versus odd-A nuclei. When all α emitters are plotted together, there is scatter about the average trend. Restricting to fixed Z and even–even (Z, N) yields smooth curves. Odd-A and odd–odd nuclei follow the same inverse trend but lie *above* the even–even lines: their half-lives are longer by factors of 2 to 10^3 at comparable Q [6]. The prominent example is ^{235}U (even Z, odd N): its long half-life ($t_{1/2} \approx 7 \times 10^8$ y) allows natural uranium to persist and thermal-neutron fission reactors to operate.

Orders of magnitude. ^{232}Th ($Q \approx 4.08\,\mathrm{MeV}$, $t_{1/2} \approx 1.4 \times 10^{10}$ y) and ^{218}Th ($Q \approx 9.85\,\mathrm{MeV}$, $t_{1/2} \approx 10^{-7}$ s) illustrate that a factor of about 2 in Q corresponds to roughly 10^{24} in $t_{1/2}$ [1, 6]. This extreme sensitivity is the central puzzle solved by Gamow's tunneling theory.

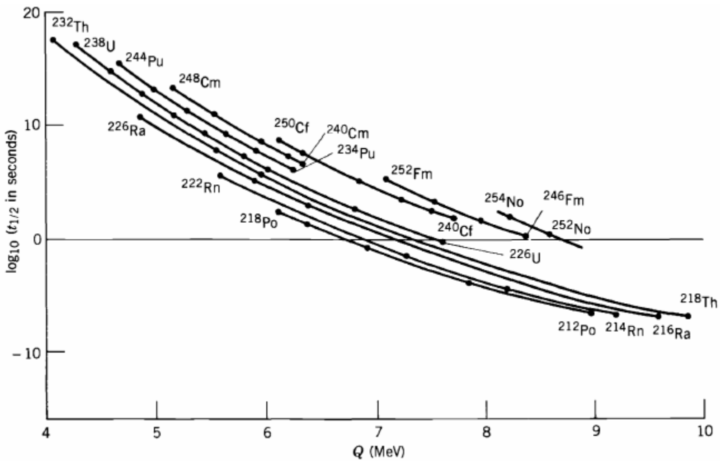

Figure 1.3: Geiger–Nuttall systematics: $\log_{10}(t_{1/2}/\mathrm{s})$ versus α-decay energy Q (MeV). Even–even nuclei form smooth curves for fixed Z [24, 6].

1.7 Toward Gamow's theory: preformation and the potential

Historical note: Gamow, Gurney, and Condon (1928)

George Gamow (1904–1968), together with Gurney and Condon, explained Geiger–Nuttall systematics by quantum tunneling of a preformed α through the Coulomb barrier [25, 26, 6, 14, 2]. The success of the one-body model does not prove that α clusters exist permanently inside heavy nuclei; it shows that decay rates behave *as if* an α were preformed at the nuclear surface.

In the Gamow model one assumes that two protons and two neutrons are already correlated as an α cluster inside the parent nucleus. The cluster moves in a potential energy $V(r)$ due to the residual nucleus, where r is the distance between their centres:

- **Nuclear well ($r < R$).** The strong force dominates. The potential is approximated by a square well of depth $V_0 \sim 30$–$40\,\mathrm{MeV}$. The Coulomb repulsion is small inside the nuclear volume and is neglected in this first approximation.
- **Coulomb barrier ($r > R$).** The nuclear force has short range; outside the surface the repulsive Coulomb potential remains:

$$V_{\mathrm{C}}(r) = \frac{(Z-2)\cdot 2e^2}{4\pi\varepsilon_0\, r} = \frac{Z_1 Z_2 e^2}{4\pi\varepsilon_0\, r}, \tag{1.31}$$

  with $Z_1 = Z - 2$ (charge of the daughter) and $Z_2 = 2$ (charge of the α).

For $\ell = 0$ the centrifugal term vanishes; $\ell \neq 0$ adds $\hbar^2\ell(\ell+1)/(2\mu r^2)$ to the barrier (Lecture 17).

Barrier height: numerical example. The Coulomb barrier height is the value of V_{C} at the effective contact distance. For $Z = 72$ and $A \approx 216$, the daughter radius is

$$R_d \approx 1.25\, A^{1/3}\,\mathrm{fm} \approx 1.25 \times 216^{1/3}\,\mathrm{fm} \approx 1.25 \times 6\,\mathrm{fm} \approx 7.5\,\mathrm{fm}. \tag{1.32}$$

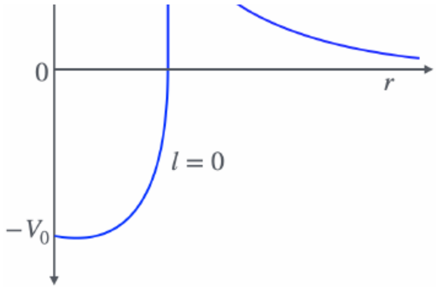

Figure 1.4: Nuclear square well joined to the Coulomb barrier $V_C(r)$ for $\ell = 0$. The horizontal line marks the available energy $E = Q$. The classically forbidden region lies between the inner radius R and the outer turning point b where $V_C(b) = Q$.

Including the α-particle radius $R_\alpha \approx 1.5\,\text{fm}$, the centre-to-centre distance at contact is

$$R \approx R_d + R_\alpha \approx 9\,\text{fm}. \tag{1.33}$$

At this separation,

$$V_C \approx \frac{2 \times (Z-2) \times e^2/(4\pi\varepsilon_0)}{R} \approx \frac{2 \times 70 \times 1.44\,\text{MeV fm}}{9\,\text{fm}} \approx 22.4\,\text{MeV}. \tag{1.34}$$

Typical α-decay Q values are only 4–9 MeV, so $Q \ll V_C(R)$: classically the α cannot escape. Quantum mechanics permits tunneling through the barrier between R and b; the calculation of the penetration probability is the subject of Lecture 17.

Takeaway

α decay in heavy nuclei is favoured by large B_α and Coulomb energy considerations ($Q > 0$ from roughly $A \sim 150$ onward in the SEMF). Observed stability through ^{208}Pb, and the extraordinary longevity of ^{209}Bi, require tunneling: $Q > 0$ is necessary but not sufficient. The Geiger–Nuttall correlation and the potential-barrier picture set the stage for the Gamow factor derived in the next chapter.

1.8 Deeper physics: Q_α and Geiger–Nuttall slopes

1.8.1 Evaluating Q_α from masses

The α-decay energy release is fixed by mass conservation. For ${}^{A}_{Z}X \to {}^{A-4}_{Z-2}Y + \alpha$,

$$Q_\alpha = [M(X) - M(Y) - M(^4\text{He})]c^2, \tag{1.35}$$

using atomic masses so that the two emitted electrons of the neutral daughter cancel with the parent atomic electrons [6, 1]. The same Q appears as the α kinetic energy in the centre-of-mass frame when recoil is neglected ($A \gg 4$). Shell and pairing corrections appear as local deviations from a smooth SEMF trend; precision work requires evaluated tables rather than the liquid-drop estimate alone [20, 21].

Numerical Q_α for ^{212}Po

Using neutral-atom masses from evaluated data, $M(^{212}\text{Po}) - M(^{208}\text{Pb}) - M(^{4}\text{He})$ gives $Q_\alpha \approx 8.95\,\text{MeV}$ and $t_{1/2} \approx 3 \times 10^{-7}\,\text{s}$ [6, 20]. Compare with ^{238}U: $Q_\alpha \approx 4.27\,\text{MeV}$ and $t_{1/2} \approx 4.5 \times 10^{9}\,\text{y}$. The higher-$Q$ isotope is shorter lived by roughly twenty-four orders of magnitude, the central puzzle of the Geiger–Nuttall plot [24, 2].

1.8.2 Reading the Geiger–Nuttall slope

Empirically, even–even α emitters of fixed Z obey (1.30). The slope a is positive: each increment in $Q^{-1/2}$ shortens the half-life. A rough Gamow estimate (Lecture 17) shows that the tunneling exponent scales as $\sqrt{\mu/Q}$ through the Coulomb turning point $b \propto 1/Q$, so $\log t_{1/2}$ varies nearly linearly with $Q^{-1/2}$ over the observed 4–9 MeV window [25, 6]. The intercept b depends primarily on Z because the barrier height grows with daughter charge. Different isotopic chains therefore form parallel lines on a $\log t_{1/2}$ versus Q plot.

The physical content is extreme sensitivity: the forbidden region width $b - R$ shrinks only as $Q^{-1/2}$ while the penetration probability falls exponentially in that width. A factor of two in Q therefore changes $t_{1/2}$ by many orders of magnitude, which is why uranium persists in nature while polonium isotopes with $Q \sim 9\,\text{MeV}$ decay in microseconds [1, 2]. The SEMF predicts a smooth $Q_\alpha(A)$ trend; shell closures near $N = 126$ and $Z = 82$ produce kinks that appear as vertical shifts on the Geiger–Nuttall plot for fixed Z [6, 20].

Remark

The Geiger–Nuttall rule is a *correlation*, not a substitute for microscopic calculation. Odd-A and odd–odd parents typically lie above the even–even curves (longer lifetimes at the same Q) because angular momentum and hindrance reduce the preformation overlap. Treating all nuclei with one line overpredicts decay rates for ^{235}U by orders of magnitude [6].

Key idea

Two observables, one exponential law. Laboratory α spectroscopy measures Q from the kinetic energy K_α; activity measurements give $t_{1/2}$. Their extreme correlation across twenty-plus decades of lifetime is explained only when quantum tunneling through the Coulomb barrier is included. Lecture 17 derives the Gamow factor that turns this empirical slope into a calculable penetration probability [14, 25].

1.8.3 Assumptions and limits of the Q_α analysis

Equation (1.35) assumes the decay proceeds to the ground state of the daughter and that recoil corrections are negligible. Decay to excited daughter states reduces the α energy by the excitation energy and splits the Geiger–Nuttall systematics into fine-structure branches [6]. Atomic-electron rearrangement after recoil contributes at the eV level and is ignored in nuclear Q tabulations [1]. For very heavy nuclei, Q_α alone does not determine the dominant decay mode: spontaneous fission competes when the fissility parameter Z^2/A exceeds the critical value of Lecture 23 [6, 54]. The Geiger–Nuttall plot remains the first diagnostic because it compresses energetics and lifetime into one figure before any microscopic model is invoked.

1.9 Further physics from the literature

Even–even systematics and hindrance. Krane emphasises that Geiger–Nuttall plots restricted to fixed Z and even–even (Z, N) form smooth curves, while odd-A and odd–odd nuclei lie systematically above those curves (longer lifetimes at the same Q) [6]. The deviation is quantified by the *hindrance factor* $F = \lambda_{\text{theory}}/\lambda_{\text{exp}}$: values near unity indicate a normal Gamow transition; $F \gg 1$ signals poor parent-daughter overlap or selection-rule suppression.

Neutron number and shell effects. Adding neutrons to a heavy isotope generally lowers Q_α and lengthens $t_{1/2}$. A pronounced discontinuity near $N = 126$ appears in $Q(A)$ plots because the daughter from α emission often sits near that closed neutron shell [6, 1]. The SEMF captures the average trend but not these local kinks; evaluated masses from [20, 21] are required for quantitative work.

Competition with other channels. For very heavy nuclei, spontaneous fission competes with α decay; the dominant mode depends on Z, A, and shell structure. Cluster radioactivity (^{14}C, ^{24}Ne, and heavier ejectiles) and proton radioactivity near the proton drip line are rare variants of the same barrier penetration physics with different charge, mass, and preformation factors [6, 1, 14].

Historical context. Rutherford's 1911 interpretation of Geiger–Marsden scattering established the nuclear atom; the same α particles from natural sources later provided discrete energy spectra that confirmed energy quantisation in nuclear decays [2, 14]. Modern silicon detectors resolve α groups to keV precision, enabling branching-ratio studies (Lecture 17).

Reading guide

Krane [6] Ch. 8 (systematics and potential model); Dunlap [1] Ch. 8 (energetics and atomic-mass conventions); Basdevant [14] Sect. 2.6 (Gamow model overview); Demtröder [2] Sect. 3.3 (historical Geiger–Nuttall plot and kinematics).

1.9.1 From Q_α systematics to tunneling (Lecture 17)

The Geiger–Nuttall plot compresses two independent measurements into one empirical law. To move from correlation to mechanism, combine the Q-value with the Coulomb turning point $b = Z_1 Z_2 e^2/(4\pi\varepsilon_0 Q)$. For fixed Z, increasing Q shrinks the classically forbidden width $b - R$ and lowers the Gamow exponent G. A back-of-the-envelope estimate for even–even nuclei uses $\log_{10} t_{1/2} \propto G/\ln 10 \propto Z_1 Z_2/\sqrt{Q}$, matching the observed $Q^{-1/2}$ slope of (1.30) [25, 6].

Slope ratio between thorium and uranium chains

On a $\log t_{1/2}$ versus $Q^{-1/2}$ plot, thorium ($Z = 90$) and uranium ($Z = 92$) even–even chains are nearly parallel but offset vertically. The offset reflects the Z-dependence of the barrier height at fixed A: higher daughter charge raises $V_C(R)$ and lengthens lifetimes at the same Q. A 2 MeV increase in Q_α typically shortens $t_{1/2}$ by ten to fifteen orders of magnitude for actinides [6, 1]. This is the quantitative content behind the qualitative Geiger–Nuttall figure in the main lecture.

1.9.2 Competition with fission and the decay chain

For $A \gtrsim 230$, spontaneous fission competes with α emission. The fissility parameter Z^2/A of Lecture 23 sets the fission barrier scale; when B_f drops below a few MeV, fission half-lives can fall below α half-lives regardless of a favourable Q_α [6, 54]. Superheavy synthesis chains terminate when neither α nor fission allows further Z increase: the same barrier-penetration language governs both channels. Cluster radioactivity (^{14}C emission from ^{223}Ra) is a rare third variant with higher Coulomb barrier and smaller preformation factor [14, 1].

Key idea

Arc through the course. α decay (Lectures 16–17) supplies the Gamow exponent reused in fusion (Lectures 25–26). Fission (Lectures 23–24) competes when Z^2/A is large. Reading a Geiger–Nuttall point together with Q_α from AME2020 and a fissility estimate is a compact summary of heavy-nucleus stability [27, 6].

1.9.3 Worked link: from Q_α to half-life orders of magnitude

Take two even–even polonium isotopes on the same $Z = 84$ chain. If $Q_1/Q_2 \approx 4$ (a factor of two in $Q^{-1/2}$), the Gamow exponent changes by roughly $\sqrt{Q_1/Q_2} - 1 \approx 100\%$ in the leading $1/\sqrt{Q}$ term, and $\log_{10}(t_{1/2})$ shifts by $\sim$ 10–15 units for typical actinide barriers [6, 25]. This is the quantitative reason that ^{218}Th ($Q \approx 9.85$ MeV, $t_{1/2} \sim 10^{-7}$ s) and ^{232}Th ($Q \approx 4.08$ MeV, $t_{1/2} \sim 10^{10}$ y) coexist on one smooth Geiger–Nuttall line. When moving to reactions, the same Q bookkeeping sets thresholds for (α, n) and (α, p) channels on light targets (Lecture 22) [14, 1].

1.9.4 Hindrance and the odd-A example

Odd-A α emitters such as ^{235}U lie above the even–even Geiger–Nuttall curves because angular momentum and poor parent-daughter overlap reduce the preformation factor [6, 1]. The hindrance factor $F = \lambda_{\text{theory}}/\lambda_{\text{exp}}$ quantifies the deviation: $F \approx 1$ for normal even–even transitions, $F \gg 1$ for suppressed ones. This is why natural uranium persists for 10^9 years despite a modest $Q_\alpha \approx 4.27$ MeV. The same overlap language reappears in transfer spectroscopic factors (Lecture 21) and in β-decay $\log ft$ values (Lecture 19) [6, 14].

1.10 Deeper reading: Q_α, Geiger–Nuttall, and preformation

Geiger–Nuttall plots correlate $\log T_{1/2}$ with $1/\sqrt{Q_\alpha}$ because the Gamow penetrability dominates the lifetime. Preformation (the many-body overlap that prepares an α particle) multiplies the attempt frequency but usually varies far less than the exponential tunneling factor. Fine structure to excited daughter states tests that overlap beyond a single ground-state branch.

Superheavy α chains (Lecture 25) use the same Q_α arithmetic with AME masses where available. Competition with fission (Lectures 23–24) terminates many chains. Compute Q_α for ^{212}Po from mass excesses once by hand: the exercise ties Lecture 4 binding differences to Lecture 17 tunneling.

Reduced widths and dimensionless hindrance

Beyond Geiger–Nuttall systematics, reduced widths compare α emission probabilities after removing the known penetrability. Small reduced widths signal poor preformation or structural mismatch with the daughter. Fine-structure branching ratios to rotational bands in deformed emitters further constrain the parent wave function.

Cluster radioactivity

Heavier cluster emission (^{14}C, etc.) is rarer but conceptually identical: Q value plus penetrability plus preformation. It reinforces that α decay is one member of a cluster family rather than an isolated miracle of $A = 4$.

Geiger–Nuttall construction

From AME masses, compute Q_α for a sequence of even–even polonium or radon isotopes and plot $\log T_{1/2}$ versus $1/\sqrt{Q_\alpha}$. Fit a straight line and note outliers. Outliers often signal hindered transitions, wrong spin assignments, or isomer contamination. The plot makes Lecture 17's exponential penetrability visible before any WKB integral is written.

Discuss preformation qualitatively: nuclei with clear α-cluster correlations may sit systematically below the average line (faster decay) after penetrability is removed. That residual is the structural content beyond Gamow's barrier factor and the bridge to microscopic cluster models used in superheavy spectroscopy.

Alpha decay links mass differences to tunneling. Geiger–Nuttall plots make the exponential visible; microscopic preformation explains residual scatter about the trend line.

In practice, rework one numerical estimate from the lecture with a different parameter set and compare the shift to the quoted experimental uncertainty. If the shift exceeds the uncertainty, the estimate is teaching a scale, not delivering a fit. That distinction keeps theoretical cartoons honest when they sit beside evaluated data tables and modern many-body calculations. Along the course arc, write one sentence linking this chapter backward and one forward: the discipline of those two sentences is as important as any single formula. Examination problems rarely ask for a literature review, but they do ask for the scale argument that literature reviews presuppose.

Synthesis problem

Write a half-page note that (i) restates the chapter's central scale or selection rule in one equation, (ii) evaluates it numerically for one concrete nucleus or energy, and (iii) names the neighbouring lecture that uses the result. Keep the note free of research-frontier speculation; the goal is fluency with the lecture physics itself. If an assumption fails (Born approximation, spherical mean field, allowed transition, one-dimensional barrier), state the failure mode in a final sentence.

That habit converts passive reading into examination-ready understanding and makes the later research-frontier box read as an extension rather than a replacement.

Research frontier: α decay, clusters, and student projects

Geiger–Nuttall systematics (Lecture 16) remain useful for quick half-life estimates, but microscopic preformation factors, cluster radioactivity, and α chains from superheavy elements are active frontiers [53]. Precision Q_α values from AME2020 and decay spectroscopy at SHE factories map shell effects near the predicted island of stability around $Z \sim 114$–126 and $N \sim 184$ [27, 51]. Competition between α emission and spontaneous fission terminates many heavy decay chains and sets practical limits on how far synthesis can be pushed. What remains uncertain includes absolute preformation probabilities, the location of the next closed shells beyond oganesson, and the reliability of extrapolated Q_α values when mass models disagree. Gamow's exponential barrier penetration still dominates the lifetime, but the many-body overlap that prepares the α particle is no longer treated as a universal constant.

Cluster radioactivity and fine-structure α branching to excited daughter states provide additional microscopic tests of preformation. When a decay chain populates both ground and excited states, the branching ratios constrain the parent wave function beyond a single Geiger–Nuttall point. That is a natural extension of the lecture systematics.

Student directions. (1) Data exercise: from AME2020, compute Q_α for ^{212}Po and ^{252}Cf and relate $\log T_{1/2}$ to $1/\sqrt{Q}$. (2) Conceptual note: sketch why a large Q_α alone does not guarantee a short half-life if the preformation factor is tiny. (3) Literature summary: summarise one recent SHE α-decay chain and its Z, N assignments [53].

1.11 Problems with solutions

Problem 16.1 — K_α fraction for $A = 220$

For α decay of a nucleus with $A = 220$, estimate the fraction of Q carried by the α particle using Eq. (1.23).

Solution 16.1

Step 1. Write the kinematic ratio from momentum conservation:

$$\frac{K_\alpha}{Q} = \frac{M_d}{M_d + M_\alpha}.$$

Step 2. Approximate masses by nucleon count: $M_d \approx (A-4)u$ and $M_\alpha \approx 4u$, so $M_d + M_\alpha \approx Au$.

Step 3. Substitute $A = 220$:

$$\frac{K_\alpha}{Q} \approx 1 - \frac{4}{A} = 1 - \frac{4}{220} = 1 - 0.01818 = 0.982.$$

The α particle carries about 98.2% of Q; the daughter recoil is about 1.8% [6, 1].

Problem 16.2 — Half-life and mean life from λ

A sample has decay constant $\lambda = 1.0 \times 10^{-6}\,\mathrm{s}^{-1}$. Find (a) the half-life $t_{1/2}$ in days, and (b) the mean life τ.

Solution 16.2

Step 1 (half-life). From Eq. (1.28):

$$t_{1/2} = \frac{\ln 2}{\lambda} = \frac{0.693}{1.0 \times 10^{-6}\,\mathrm{s}^{-1}} = 6.93 \times 10^5\,\mathrm{s}.$$

Step 2 (convert to days).

$$t_{1/2} = \frac{6.93 \times 10^5}{86400\,\mathrm{s/day}} \approx 8.0\,\mathrm{days}.$$

Step 3 (mean life).

$$\tau = \frac{1}{\lambda} = \frac{1}{1.0 \times 10^{-6}} = 1.0 \times 10^6\,\mathrm{s} \approx 11.6\,\mathrm{days}.$$

Note $\tau = t_{1/2}/\ln 2 \approx 1.443\,t_{1/2}$.

Problem 16.3 — Activity decay over three half-lives

At $t = 0$ a source has activity $\mathcal{A}_0 = 3.7 \times 10^4\,\mathrm{Bq}$ (1 mCi). What is the activity after $3\,t_{1/2}$?

Solution 16.3

Step 1. Activity follows Eq. (1.29): $\mathcal{A}(t) = \mathcal{A}_0\,e^{-\lambda t}$.

Step 2. After one half-life, $\mathcal{A}$ falls by a factor of 2. After three half-lives:

$$\mathcal{A}(3t_{1/2}) = \frac{\mathcal{A}_0}{2^3} = \frac{\mathcal{A}_0}{8}.$$

Step 3. Numerical value:

$$\mathcal{A}(3t_{1/2}) = \frac{3.7 \times 10^4}{8} = 4.6 \times 10^3\,\mathrm{Bq}.$$

Problem 16.4 — Coulomb barrier height for $Z = 92$

Estimate the Coulomb barrier height for α decay of $^{238}\mathrm{U}$ ($Z = 92$, $A = 238$) using $R_d = 1.25A^{1/3}\,\mathrm{fm}$ and $R_\alpha = 1.5\,\mathrm{fm}$. Compare with typical $Q \approx 4.3\,\mathrm{MeV}$.

Solution 16.4

Step 1 (daughter radius).

$$R_d = 1.25 \times 238^{1/3}\,\mathrm{fm} \approx 1.25 \times 6.20\,\mathrm{fm} \approx 7.75\,\mathrm{fm}.$$

Step 2 (contact distance).

$$R = R_d + R_\alpha \approx 7.75 + 1.5 = 9.25\,\mathrm{fm}.$$

Step 3 (barrier height). With $Z_1 = Z - 2 = 90$:

$$V_\mathrm{C}(R) = \frac{2 \times 90 \times 1.44\,\mathrm{MeV\,fm}}{9.25\,\mathrm{fm}} \approx 28\,\mathrm{MeV}.$$

Step 4 (comparison). $Q \approx 4.3\,\mathrm{MeV} \ll 28\,\mathrm{MeV}$, so the decay proceeds only by quantum tunneling. The ratio $Q/V_\mathrm{C} \sim 0.15$ explains the enormous half-life ($\sim 4.5 \times 10^9\,\mathrm{y}$) [6, 20].

Problem 16.5 — Geiger–Nuttall estimate

Two even–even isotopes of the same element have α energies $Q_1 = 5.0\,\mathrm{MeV}$ and $Q_2 = 6.0\,\mathrm{MeV}$. If the first has $t_{1/2}^{(1)} = 10^6\,\mathrm{s}$, estimate $t_{1/2}^{(2)}$ using $\log_{10} t_{1/2} = aQ^{-1/2} + b$ with the same a, b.

Solution 16.5

Step 1. Subtract the two Geiger–Nuttall equations:

$$\log_{10} t_{1/2}^{(2)} - \log_{10} t_{1/2}^{(1)} = a\left(Q_2^{-1/2} - Q_1^{-1/2}\right).$$

Step 2. A Geiger–Nuttall plot of $\log_{10} t_{1/2}$ against $Q^{-1/2}$ has a *positive* slope: larger $Q^{-1/2}$ means a lower decay energy and a longer half-life. For a representative heavy isotopic chain, take $a \approx +140\,\mathrm{MeV}^{1/2}$ (the fitted value depends on Z).

$$Q_2^{-1/2} - Q_1^{-1/2} = \frac{1}{\sqrt{6.0}} - \frac{1}{\sqrt{5.0}} = 0.4082 - 0.4472 = -0.039.$$

$$\log_{10} \frac{t_{1/2}^{(2)}}{t_{1/2}^{(1)}} \approx +140 \times (-0.039) \approx -5.46.$$

Step 3.

$$t_{1/2}^{(2)} \approx 10^6 \times 10^{-5.46} \approx 3.5\,\mathrm{s}.$$

A 20% increase in Q therefore shortens the estimated half-life by about 3×10^5. The numerical value is only illustrative because a must be fitted for the isotopic chain, but the sign and exponential sensitivity are unambiguous [6, 1].

Bibliography

[1] R. A. Dunlap, *An Introduction to the Physics of Nuclei and Particles* (2nd ed.), IOP Publishing, Bristol (2023), DOI: 10.1088/978-0-7503-6094-4, Ch. 3 (Nuclear composition and size).

[2] W. Demtröder, *Nuclear and Particle Physics*, Undergraduate Lecture Notes in Physics, Springer, Cham (2023).

[3] S. Petrera, *Problems and Solutions in Nuclear and Particle Physics*, UNITEXT for Physics, Springer, Cham (2019).

[4] F. Terranova, *A Modern Primer in Particle and Nuclear Physics*, Oxford University Press (2021).

[5] S. D'Auria, *Introduction to Nuclear and Particle Physics*, Undergraduate Lecture Notes in Physics, Springer, Cham (2018).

[6] K. S. Krane, *Introductory Nuclear Physics*, Wiley, New York (1988).

[7] R. Hofstadter, "Electron scattering and nuclear structure," Rev. Mod. Phys. **28**, 214 (1956).

[8] H. F. Ehrenberg, R. Hofstadter, U. Meyer-Berkhout, D. G. Ravenhall, and S. E. Sobottka, "High-Energy Electron Scattering and the Charge Distribution of Carbon-12 and Oxygen-16," Phys. Rev. **113**, 666 (1959).

[9] H. Yukawa, "On the interaction of elementary particles. I," Proc. Phys.-Math. Soc. Japan **17**, 48 (1935).

[10] R. D. Woods and D. S. Saxon, "Diffuse surface optical model for nucleon-nuclei scattering," Phys. Rev. **95**, 577 (1954).

[11] H. G. J. Moseley, "The high-frequency spectra of the elements," Phil. Mag. **26**, 1024 (1913); **27**, 703 (1914).

[12] C. F. von Weizsäcker, "Zur Theorie der Kernmassen," Z. Phys. **96**, 431 (1935).

[13] P. Cappellaro, *Introduction to Applied Nuclear Physics* (MIT OpenCourseWare / LibreTexts), CC BY-NC-SA 4.0.

[14] J.-L. Basdevant, J. Rich, and M. Spiro, *Fundamentals in Nuclear Physics: From Nuclear Structure to Cosmology*, Springer, New York (2005).

[15] D. Tong, *Particle Physics*, Lecture notes (University of Cambridge / CERN school notes).

[16] M. G. Mayer, "On closed shells in nuclei. II," Phys. Rev. **75**, 1969 (1949).

[17] O. Haxel, J. H. D. Jensen, and H. E. Suess, "On the "magic numbers" in nuclear structure," Phys. Rev. **75**, 1766 (1949).

[18] T. Schmidt, "Über die magnetischen Momente der Atomkerne," Z. Phys. **106**, 358 (1937).

[19] L. W. Nordheim, "On spins, moments, and shells in nuclei," Phys. Rev. **78**, 294 (1950).

[20] Evaluated Nuclear Structure Data File (ENSDF), National Nuclear Data Center, Brookhaven National Laboratory, `https://www.nndc.bnl.gov/ensdf/`.

[21] NuDat 3, National Nuclear Data Center, Brookhaven National Laboratory, `https://www.nndc.bnl.gov/nudat3/`.

[22] N. J. Stone, "Table of nuclear magnetic dipole and electric quadrupole moments," At. Data Nucl. Data Tables **90**, 75 (2005); updated compilations at NNDC.

[23] W. N. Cottingham and D. A. Greenwood, *An Introduction to Nuclear Physics* (2nd ed.), Cambridge University Press, Cambridge (2001).

[24] H. Geiger and J. M. Nuttall, "The ranges of the α particles from the radioactive substances," Phil. Mag. **22**, 613 (1911).

[25] G. Gamow, "Zur Quantentheorie des Atomkernes," Z. Phys. **51**, 204 (1928).

[26] R. W. Gurney and E. U. Condon, "Wave mechanics and radioactive disintegration," Nature **122**, 439 (1928); Phys. Rev. **33**, 127 (1929).

[27] M. Wang, W. J. Huang, F. G. Kondev, G. Audi, and S. Naimi, "The AME 2020 atomic mass evaluation (II). Tables, graphs and references," Chin. Phys. C **45**, 030003 (2021).

[28] Laboratoire National Henri Becquerel (LNHB), Recommended decay data, `http://www.lnhb.fr/nuclear-data/nuclear-data-table/`.

[29] L. M. Langer, R. D. Moffat, and H. C. Price, Jr., "Low energy beta-ray spectra: P^{32} and Cu^{64}," Phys. Rev. **76**, 1725 (1949).

[30] L. M. Langer and H. C. Price, Jr., "Shapes of the beta-spectra of the forbidden transitions of Sb^{124}, Rb^{86}, Sr^{89}, Y^{91}, and Cs^{137}," Phys. Rev. **75**, 1769 (1949).

[31] D. C. Camp and L. M. Langer, "The shape of the ^{66}Ga positron spectrum and the contribution from $0^+ \to 0^+$ transitions," Phys. Rev. **129**, 1782 (1963).

[32] H. C. Verma, *Nuclear Physics: Fundamentals and Applications*, NPTEL/IIT Kanpur lecture series, `https://hcverma.in/ncl_phy_lectures`.

[33] International Atomic Energy Agency, *LiveChart of Nuclides*, evaluated structure, decay, reaction, and fission-yield data, `https://www-nds.iaea.org/relnsd/vcharthtml/VChartHTML.html`.

[34] T. Kibédi, T. W. Burrows, M. B. Trzhaskovskaya, P. M. Davidson, and C. W. Nestor, Jr., "Evaluation of theoretical conversion coefficients using BrIcc," Nucl. Instrum. Methods Phys. Res. A **589**, 202 (2008), DOI: 10.1016/j.nima.2008.02.051.

[35] D. A. Brown *et al.*, "ENDF/B-VIII.0: The 8th major release of the nuclear reaction data library with CIELO-project cross sections, new standards and thermal scattering data," Nucl. Data Sheets **148**, 1 (2018), DOI: 10.1016/j.nds.2018.02.001.

[36] B. Acharya *et al.*, "Solar fusion III: New data and theory for hydrogen-burning stars," Rev. Mod. Phys. **97**, 035002 (2025), DOI: 10.1103/8lm7-gs18.

[37] S. N. Ghoshal, "An experimental verification of the theory of compound nucleus," Phys. Rev. **80**, 939 (1950), DOI: 10.1103/PhysRev.80.939.

[38] D. Adhikari *et al.* (PREX Collaboration), "Accurate determination of the neutron skin thickness of ^{208}Pb through parity-violation in electron scattering," Phys. Rev. Lett. **126**, 172502 (2021), DOI: 10.1103/PhysRevLett.126.172502.

[39] B. T. Reed, F. J. Fattoyev, C. J. Horowitz, and J. Piekarewicz, "Implications of PREX-II on the equation of state of neutron-rich matter," Phys. Rev. Lett. **126**, 172503 (2021), DOI: 10.1103/PhysRevLett.126.172503.

[40] B. Hu *et al.*, "Ab initio predictions link the neutron skin of ^{208}Pb to nuclear forces," Nature Phys. **18**, 1196 (2022), DOI: 10.1038/s41567-022-01715-8.

[41] E. Epelbaum, H.-W. Hammer, and U.-G. Meißner, "Modern theory of nuclear forces," Rev. Mod. Phys. **81**, 1773 (2009), DOI: 10.1103/RevModPhys.81.1773.

[42] H.-W. Hammer, S. König, and U. van Kolck, "Nuclear effective field theory: Status and perspectives," Rev. Mod. Phys. **92**, 025004 (2020), DOI: 10.1103/RevModPhys.92.025004.

[43] T. Otsuka, A. Gade, O. Sorlin, T. Suzuki, and Y. Utsuno, "Evolution of shell structure in exotic nuclei," Rev. Mod. Phys. **92**, 015002 (2020), DOI: 10.1103/RevModPhys.92.015002.

[44] H. Hergert, S. K. Bogner, T. D. Morris, A. Schwenk, and K. Tsukiyama, "The in-medium similarity renormalization group: A novel ab initio method for nuclei," Phys. Rep. **621**, 165 (2016), DOI: 10.1016/j.physrep.2015.12.007.

[45] J. M. Lattimer and M. Prakash, "The equation of state of hot, dense matter and neutron stars," Phys. Rep. **621**, 127 (2016), DOI: 10.1016/j.physrep.2015.12.005.

[46] J. M. Lattimer, "Neutron stars and the nuclear matter equation of state," Annu. Rev. Nucl. Part. Sci. **71**, 433 (2021), DOI: 10.1146/annurev-nucl-102419-124827.

[47] B. P. Abbott *et al.* (LIGO Scientific Collaboration and Virgo Collaboration), "GW170817: Observation of gravitational waves from a binary neutron star inspiral," Phys. Rev. Lett. **119**, 161101 (2017), DOI: 10.1103/PhysRevLett.119.161101.

[48] M. J. Dolinski, A. W. P. Poon, and W. Rodejohann, "Neutrinoless double-beta decay: Status and prospects," Annu. Rev. Nucl. Part. Sci. **69**, 219 (2019), DOI: 10.1146/annurev-nucl-101918-023407.

[49] M. Agostini, G. Benato, J. A. Detwiler, J. Menéndez, and F. Vissani, "Toward the discovery of matter creation with neutrinoless $\beta\beta$ decay," Rev. Mod. Phys. **95**, 025002 (2023), DOI: 10.1103/RevModPhys.95.025002.

[50] P. Gysbers *et al.*, "Discrepancy between experimental and theoretical β-decay rates resolved from first principles," Nature Phys. **15**, 428 (2019), DOI: 10.1038/s41567-019-0450-7.

[51] H. L. Crawford, K. Fossez, S. König, and A. Spyrou, "A vision for the science of rare isotopes," Annu. Rev. Nucl. Part. Sci. **74**, 141 (2024), DOI: 10.1146/annurev-nucl-121423-091501.

[52] Nuclear Science Advisory Committee, *A New Era of Discovery: The 2023 Long Range Plan for Nuclear Science*, U.S. Department of Energy and National Science Foundation (2023), `https://nuclearsciencefuture.org/`.

[53] S. A. Giuliani, Z. Matheson, W. Nazarewicz, E. Olsen, P.-G. Reinhard, J. Sadhukhan, B. Schuetrumpf, N. Schunck, and P. Schwerdtfeger, "Colloquium: Superheavy elements: Oganesson and beyond," Rev. Mod. Phys. **91**, 011001 (2019), DOI: 10.1103/RevModPhys.91.011001.

[54] N. Schunck and D. Regnier, "Theory of nuclear fission," Prog. Part. Nucl. Phys. **125**, 103963 (2022), DOI: 10.1016/j.ppnp.2022.103963.

[55] I. Counts, J. Hur, D. P. L. Aude Craik, H. Jeon, C. Leung, J. C. Berengut, A. Geddes, A. Kawasaki, W. Jhe, and V. Vuletić, "Evidence for nonlinear isotope shift in Yb^+ search for new boson," Phys. Rev. Lett. **125**, 123002 (2020), DOI: 10.1103/PhysRevLett.125.123002.

[56] I. Angeli and K. P. Marinova, "Table of experimental nuclear ground state charge radii: An update," At. Data Nucl. Data Tables **99**, 69 (2013), DOI: 10.1016/j.adt.2011.12.006.

[57] S. Kraemer *et al.*, "Observation of the radiative decay of the ^{229}Th nuclear clock isomer," Nature **617**, 706 (2023), DOI: 10.1038/s41586-023-05894-z.